# Self-preservation in annular jet with large diameter ratio

Arezki Bouha, Émilien Varea, Béatrice Patte-Rouland, Luminita Danaila

# Self-preservation in annular jet with large diameter ratio

**A. BOUHA[a] , E. VAREA , B. PATTE-ROULAND and L. DANAILA.**

CNRS UMR 6614 - CORIA. Normandie Université.
(a) arezki.bouha@coria.fr

## Résumé

*Cette étude vise à comprendre et quantifier l'influence des structures cohérentes sur les petites échelles turbulentes dans un jet annulaire à fort rapport de diamètres. Ce type de jet est représentatif des géométries de type "bluff-body" largement utilisées en combustion [24]. On s'intéresse, dans un cas d'un jet faiblement chauffé, à l'évolution axiale des quantités moyennes de vitesse, $\bar{U}$, et de dissipation de l'énergie cinétique, $\bar{\epsilon}$, ainsi que des quantités moyennes de scalaire passif associées, $\bar{\theta}$ et $\bar{\chi}$.*

## Abstract

*Considering an annular jet with a large diameter ratio, this study aims at understanding and quantifying the influence of coherent structures on turbulent small scales. This typical geometry is close to those widely used in combustion processes, "bluff-body", which is useful for flame stabilization enhancement [24]. For the investigated flow which is slightly heated, we are interested in the evolution of mean values of velocity $\bar{U}$ and passive scalar $\bar{\theta}$ along the jet axis. Particular attention will be paid to the evolution of the energy and scalar dissipation rates, $\bar{\epsilon}$ and $\bar{\chi}$, respectively.*

**Annular jet, Coherent structures, Velocity decay, Scalar, Dissipation rate.**

## 1 Introduction

Annular jets are widely used in industrial processes. They are known for their ability to mix inlet flow with the surrounding on relatively short distances compared to standard jets. Considering combustion processes, this specific geometry, called "bluff-body", allows a better stabilization of the flame and therefore reduces combustion pollutant emissions [24]. In the case of exhaust fan

or chimney, the jet plume is reduced. The dilution of pollutants is enhanced which decreases the risk of high concentration pollutant pockets transported by wind [6].
Similarly to classical round jets, annular jet topology can be divided into 3 parts: i) the initial zone, ii) the intermediate zone and iii) the fully developed zone. Based on the analysis of similarity curves of the mean velocity and turbulence intensity quantities [18], the similarity regime is reached on shorter distances downstream the jet nozzle compared to round jets. Moreover, this geometry significantly affect the initial conditions and coherent structures are preferentially generated in the intermediate zone. It has been shown that coherent structures significantly alter the energy transfer to the small dissipative scales, as observed in shear flows [28], grid turbulence configurations [13] or weak flows [14]. To the author knowledge, it is worth noting that there has been no previous attempt to assess the scalar behavior in annular jet flows. Therefore, this study aims at evaluating the mean values of velocity $\bar{U}$ and scalar $\bar{\theta}$ along the jet axis. Particular attention is paid to the evolution of the kinetic energy and scalar dissipation rates, $\bar{\epsilon}$ and $\bar{\chi}$, respectively.
The paper is organized as follows. In Sec. 2, the experimental configuration, conditions and measurements apparatus are presented. In Sec. 3, the decay rate of mean velocity and scalar, and their respective dissipation rates are estimated and compared to classical round jets. Finally, the main results are summarized and perspectives on further work are described.

# 2 Experimental setup

## 2.1 Experimental Configuration

A schematic of the annular jet is shown in Fig. 1. The annular jet is fed with air from the bottom through symmetrical inlets. The air is previously heated up to 11°C above the ambient temperature to generate a temperature gradient. To get as close as possible to a top-hat velocity profile at the nozzle exit, prior to the convergent which has a specific contraction ratio [12], the flow passes through honeycomb cells. The outlet nozzle is characterized by an outer diameter $D_0 = 53.88\ mm$, and an inner diameter $D_i = 48.75\ mm$. The inner disk thickness is $e = 2.56\ mm$. The diameter ratio, $\zeta = \frac{D_0}{D_i} = 0.91$, is significantly higher than that used in Ko and Chan [18] or than that of Warda et al. [28] which are $\zeta = 0.45$ and $\zeta = 0.71$, respectively. However, the diameter ratio is close to the one found in Aly et al. [2] where $\zeta$ value is 0.96. As mentioned in [18], increasing the diameter ratio reduces the reattachment distance.

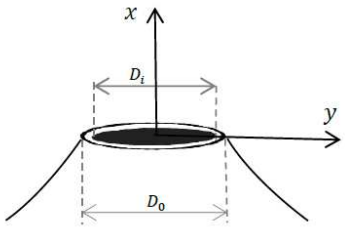


Figure 1: Schematic of an annular jet nozzle of outer diameter $D_0$ and inner diameter $D_i$.

## 2.2 Experimental Conditions

The jet exit velocity $U_0$ is set to 10 $m/s$ which results in a Reynolds number (based on the outside diameter) of $Re_{D_0} = 3.45\ 10^4$ ($Re_{D_0} = \frac{U_0 D_0}{\nu}$). The measurements are performed along the annular jet axis, between $\frac{x}{D_0} = 2$ and $\frac{x}{D_0} = 9$. As mentioned earlier, the exit temperature $\theta_0$ is set to 11°C above the ambient temperature. Therefore to evaluate the effect of buoyancy to inertial forces, one can define the ratio $\frac{Gr}{Re^2}$, where $Gr$ is the Grashof number. In this study, the ratio $\frac{Gr}{Re^2}$ is about 0.002 which is close to the value in Antonia and Mi [3]. This result implies that the buoyancy forces can be neglected compared to the inertial forces. Therefore, the temperature can be treated as a passive contaminant scalar.

## 2.3 Measurement devices

Simultaneous measurements of velocity and scalar quantities are performed. Using X-probe wire operating at a constant temperature (CTA), we evaluated the axial and radial velocity components $u$ and $v$, respectively. The probe is made of 5.04 $\mu m$ diameter Wollaston wires ($Pt - 10\%Rd$). The active length/diameter ratio is about 200 and the CTA circuit operates at an overheat ratio of 1.4. The X-probe calibration is carried out using the lookup table method (LUT) as reported in Burattini and Antonia [8].
Temperature fluctuations $\theta$ are evaluated with a constant current anemometer (CCA), operating at low overheat ratio (cold wire). The later is made of 0.64 $\mu m$ diameter Wollaston wire and the active length/diameter ratio is about 880. Browe and Anonia [7] showed that for active length/diameter ratios lower than 1500, errors due to the heat conduction between prongs could affect the temperature momentum and its time derivative calculation. Otherwise reducing the active length/diameter ratio reduces the spatial resolution. Therefore, the same strategy as described in Lemay and Benaïssa [19] is chosen. The authors recommended ratios between 700 and 1000. As suggested by Paranthoën and

| $x/D_0$ | 3 | 7 |
|---|---|---|
| $\overline{\theta}$ $(°C)$ | 31.04 | 28.56 |
| $R_\lambda$ | 141 | 118 |
| $\overline{U}$ $(m/s)$ | 4.72 | 2.36 |
| $\eta$ $(mm)$ | 0.097 | 0.134 |
| $\eta_\theta$ $(mm)$ | 0.116 | 0.214 |
| $l_{w1}/\eta$ | 10.4 | 7.5 |
| $l_{w1}/\eta_\theta$ | 4.78 | 2.59 |
| $f_s$ $(10^3 HZ)$ | 28.05 | 11.65 |
| $f_K$ $(10^3 HZ)$ | 7.75 | 2.81 |
| $f_{K\theta}$ $(10^3 HZ)$ | 6.48 | 1.76 |

Table 1: Experimental conditions determined at the axial positions $\frac{x}{D_0} = 3, 7$.

Lecordier [22], the cold wire is totally etched which allows a better time resolution.
The configuration for the X-probe velocity sensors/wires is chosen according to Vukoslavčević and Wallace [27]. The X-probe velocity sensors are positioned along the $(x, y)$ plane and the temperature sensor is moved upstream perpendicular to the $(x, y)$ plane. This configuration avoids eventual contamination of cold wire due to the hot wires. In order to correct the instantaneous velocity voltage signals for the influence of temperature fluctuations [11], the following correction procedure is applied:

$$E^2 \frac{\theta_w - \theta_a}{\theta_w - \theta_i} = E_{corr}^2, \tag{1}$$

where $E$ and $E_{corr}$ are the instantaneous and corrected velocity voltages, respectively. $\theta_w$ and $\theta_i$ are the hot wire temperature and instantaneous temperatures, respectively. During the signal conditioning, a butterworth low pass-filter (cut-off frequency $-48db/dec$) is used in order to avoid spectral refolding of the frequencies higher than the half of the sampling frequency $f_s$. From $10^6$ to 8 $10^6$ samples are acquired at each position using a 12 bit A/D converter. The experimental conditions at $\frac{x}{D_0} = 3$ and 7 positions are summarized in Table (1). $\overline{U}$ and $\overline{\theta}$ are the local mean velocity and temperature, respectively. $R_\lambda = u'\lambda/\nu$ is the Reynolds number based on the Taylor micro-scale $\lambda$ $\left(\lambda = \overline{u^2}/\overline{(\delta u/\delta x)^2}\right)$. The longitudinal r.m.s velocity is denoted $u'$ and $\nu$ is the kinematic viscosity. The longitudinal derivative quantities are determined using the Taylor hypothesis. $\eta_\theta$ is the temperature Taylor micro-scale ($\eta_\theta = \eta/Pr^{4/3}$), where $Pr$ ($Pr = (\nu/\alpha)$) is the Prandtl number and $\alpha$ is the thermal diffusivity. $f_K$ ($f_K = \overline{U}/2\pi\eta$) is the Kolmogorov frequency and $f_{K\theta}$ ($f_{K\theta} = \overline{U}/2\pi\eta_\theta$) is the temperature micro-scale frequency.

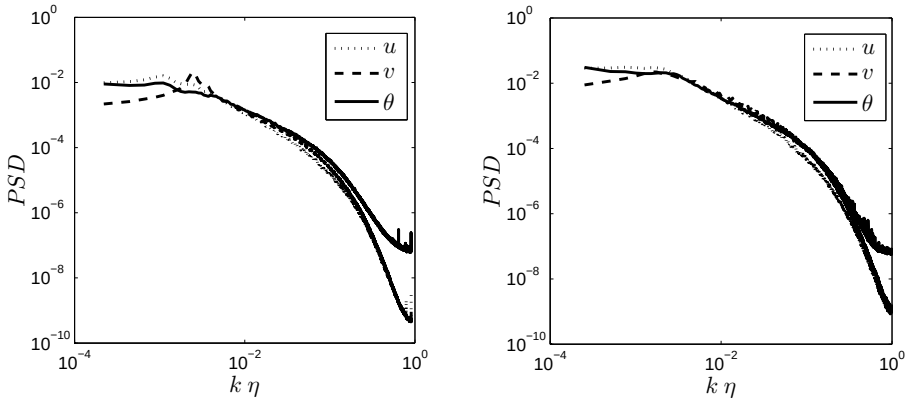


Figure 2: Power spectra of velocity components ($u$, $v$) and temperature ($\theta$). Left: $\frac{x}{D_0} = 3$. Right: $\frac{x}{D_0} = 7$.

# 3 Results and discussion

## 3.1 Spectral analysis

Figure 2 shows the velocity and temperature spectrum functions, using the Kolmogorov scaling ($\eta = (\nu^3/\overline{\epsilon})^{1/4}$). It appears that the large scale behavior is different considering the radial ($v$) or longitudinal ($u$) directions. This reflects the eventual large scale anisotropy. In the intermediate zone at $\frac{x}{D_0} = 3$, the pick in the radial velocity spectrum is linked to the presence of coherent (large scale) structures generated by the central part of the annular jet. It is well-known that $v$ is more sensitive to the coherent motion than $u$, as mentioned in [21, 4]. The pick vanishes at $\frac{x}{D_0} = 7$ resulting from flow development. At low wave numbers most part of the energy is contained in the longitudinal direction. Similarly to classical round jet configurations, the energy is transfered from the mean motion $\overline{u^2}$ to $\overline{v^2}$ as described in [29].

## 3.2 Similarity thought along the annular jet centerline

Beyond the fully developed zone, the jet seems to behave as classical round jets. One can define an equivalent jet which exhibits the same outlet velocity $U_0$ but with an equivalent diameter $D_{eq} = \sqrt{D_0^2 - D_i^2}$ based on the conservation of the mass flow rate. The mean velocity and temperature decays follow the relations,

$$\frac{\overline{U}}{U_0} = A_{\overline{U}} \left( \frac{x - x_0}{D_{eq}} \right)^{-1}, \tag{2}$$

$$\frac{\overline{\theta}-\theta_a}{\theta_0-\theta_a}=A_{\overline{\theta}}\left(\frac{x-x_0}{D_{eq}}\right)^{-1}, \tag{3}$$

The coefficients values, $A_{\overline{U}}$ and $A_{\overline{\theta}}$ are 4.8 and 4, respectively. For round jets, it appears that $5.8 \leq A_{\overline{U}} \leq 6$ [9, 10, 1, 16] and $A_{\overline{\theta}} = 4.35$ [10]. Pitts [23] established a compendium of $A_{\overline{\theta}}$ values found in the literature for a variety of measurements methods. The average value obtained was close to 4.76. The virtual origin $x_0$ was evaluated thought a linear fit of $U_0/\overline{U}$.
To evaluate the small scale processes, the axial evolution of the mean dissipation rate of the kinetic energy $\overline{\epsilon}$ and the mean dissipation rate of the temperature fluctuations $\overline{\chi}$ are calculated, Fig. 3. Note that mean quantities of velocity and temperature are also shown in Fig 3. According to [9, 15], assuming local axisymmetry seems more reliable than assuming local isotropy. Therefore, the expression of $\overline{\epsilon_{hom}}$ considering homogeneity yields

$$\overline{\epsilon}_{hom}=3\nu\overline{\left(\left(\frac{\partial u}{\partial x}\right)^2+2\left(\frac{\partial v}{\partial x}\right)^2\right)}, \tag{4}$$

The normalized mean dissipation rates follow the power law $x^{-4}$, such that

$$\frac{\overline{\epsilon}D_{eq}}{U_0^3}=A_{\overline{\epsilon}}\left(\frac{x-x_0}{D_{eq}}\right)^{-4}, \tag{5}$$

$$\frac{\overline{\chi}D_{eq}}{U_0\left(\theta_0-\theta_a\right)^2}=A_{\overline{\chi}}\left(\frac{x-x_0}{D_{eq}}\right)^{-4}. \tag{6}$$

Coefficient values for $A_{\overline{\epsilon}}$ and $A_{\overline{\chi}}$ are 32 and 6 for $Re_{D_{eq}} = 1.47\ 10^4$, respectively. For round jets, the mean dissipation rate of the energy is found to be close to 42.5 for $Re_D = 11.3\ 10^4$ and 48 for $Re_D = 12\ 10^4$ [25]. For the scalar it is close to 14.9 for $Re_D = 15\ 10^4$ [20].

Considering similarity, the mean equilibrium field is reached slightly before $x = 7D_{eq}$, Fig. 3. To make the comparison possible with round jets, $x = 7D_{eq}$ corresponds to $x = 4D_{eq}$ while plotting the normalized mean statics over $x/D_{eq}$. For round jets it takes 4 to 8 diameters [10, 28, 5]. However, mean quantities are not sensitive enough to indicate whether similarity is reached [10]. Scalar and velocity r.m.s equilibrium (results are not shown in this paper) is reached after $x = 9.4D_{eq}$ which is clearly before round jets, from 20 to 40 diameters [10, 20, 28, 29, 1]. Small dissipative scales need more distance to reach equilibrium – obtained at $x = 12D_{eq}$. It is worth noting that for round jets, distances of 26 diameters are generally reported for dissipative scales equilibrium [20].The results are summarized in Table (2).

It appears that the axial decay of mean statistics and dissipation rate are more pronounced for scalar than for dynamic field. This result is consistent with the radial transport mechanisms of momentum and heat which is higher for the

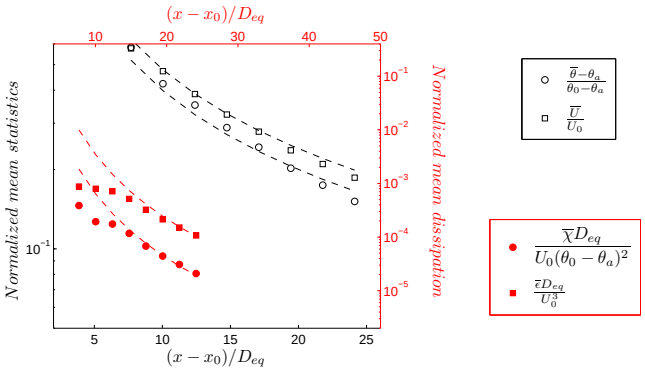


Figure 3: The longitudinal decay of Mean and dissipative quantities.

| Similarity of | Annulat jet | Round jets |
|---|---|---|
| Mean statistics | $4D_{eq}$ | $4D$ *to* $8D$ |
| R.M.S | $9.5D_{eq}$ | $20D$ *to* $40D$ |
| Dissipative scales | $12D_{eq}$ | $26D$ |

Table 2: Distance taken in annular and round jets to reach the similarity.

scalar component as shown in Fig. 4, evaluated at $\frac{x}{D_0} = 7$. The explanation of the observed accelerated flow development is intimately related to the intermediate zone which is populated by coherent structures. It has been shown for shear flows that the vorticity created after mean field instability initiates other instabilities which are responsible for the energy cascade to smaller scales [14]. For grid turbulence, it has been suggested by [13] that the self-similarity decay is due to the singular development of vortical structures randomly distributed across the flow. For wake flow [26], one can observe temporal periodicity of coherent structures which affect the turbulent scales thought phase accelerated energy transfer cascades. The differences observed between the decay rates of the measured quantities and those of round jet highlight the non-universality of self-similarity between these two types of flows. As mentioned by George [14], self-similarity depends on initial conditions. Therefore, in annular jet flows, one can say that due to initial conditions, a multiplicity of scales – large scales and specifically small scales – are generated on relatively short distances. As reported by George [14], Kerr [17] suggested that the large scale evolution is itself the energy cascade.

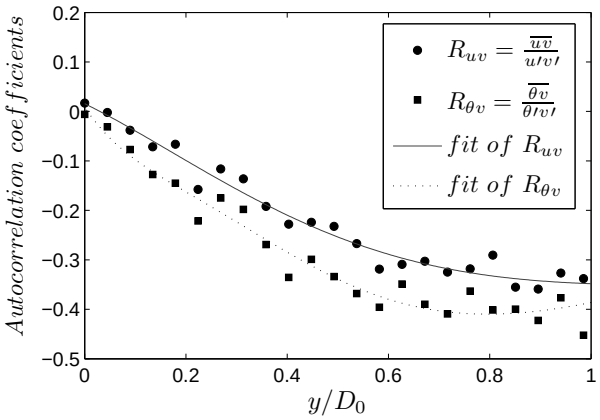


Figure 4: Radial evolution of autocorrelation coefficients.

# 4 Conclusion and perspectives

Scalar and energy behaviors in an annular jet with large diameter ratio are assessed. The decay of mean and dissipative statistics is evaluated and compared to the classical round jets. This specific geometry which generates coherent structures, leads to an establishment of a self-preserving zone on a short distance beyond the outlet jet. In perspective, we will evaluate the self-preservation trough a scale-by-scale budget, which a very restrictive test. We will also investigate the influence of the coherent structures on the turbulent cascade. Actually, we are performing a simultaneous PIV (Particle Imagery Velocimetry) and PLIF (Planar Laser Induced Fluorescence) to understand and quantify the coherent structure influence on the mixing mechanisms.

# References

[1] A. A. Abdel-Rahman, W. Chakroun, and S. F. Al-Fahed. LDA measurements in the turbulent round jet. *Mechanics Research Communications*, 24(3):277–288, 1997.

[2] M. S. Aly and M. I. I. Rashed. Experimental investigation of an annular jet. *Journal of Wind Engineering and Industrial Aerodynamics*, 37(2):155–166, 1991.

[3] R. A. Antonia and J. Mi. Temperature dissipation in a turbulent round jet. *Journal of Fluid Mechanics*, 250:531–551, 1993.

[4] R. A. Antonia, T. Zhou, and G. P. Romano. Small-scale turbulence characteristics of two-dimensional bluff body wakes. *Journal of Fluid Mechanics*, 459:67–92, 2002.

[5] P. Bradshaw, D. H. Ferriss, and R. F. Johnson. Turbulence in the noise-producing region of a circular jet. *Journal of Fluid Mechanics*, 19:591–624, 1964.

[6] M. Brendel. CFD analysis of laboratory exhaust fans and applications. In *Ashrae winter annual meeting, Atlantic City, NJ*, 2002.

[7] L. W. B. Browne and R. A. Antonia. The effect of wire length on temperature statistics in a turbulent wake. *Experiments in Fluids*, 5(6):426–428, 1987.

[8] P. Burattini and R. A. Antonia. The effect of different x-wire calibration schemes on some turbulence statistics. *Experiments in Fluids*, 38(1):80–89, 2005.

[9] P. Burattini, R. A. Antonia, and L. Danaila. Similarity in the far field of a turbulent round jet. *Physics of Fluids*, 17(2), 2005.

[10] L. P. Chua and R. A. Antonia. The turbulent interaction region of a circular jet. *International Communications in Heat and Mass Transfer*, 13(5):545–558, 1986.

[11] L. Danaila, F. Anselmet, T. Zhou, and R. A. Antonia. A generalization of yaglom's equation which accounts for the large-scale forcing in heated decaying turbulence. *Journal of Fluid Mechanics*, 391:359–372, 1999.

[12] A. Danlos. *Dynamique des jets contrôlés : Application à l' étude du mélange dans des écoulements de jets annulaires à très grand rapport de diamètres.* PhD thesis, Université de Rouen, 2009.

[13] W. K. George. The decay of homogeneous isotropic turbulence. *Physics of Fluids A: Fluid Dynamics (1989-1993)*, 4(7):1492–1509, 1992.

[14] W. K. George and R. Arndt. *Advances in turbulence.* Hemisphere Publishing Corporation, 1989.

[15] W. K. George and H. J. Hussein. Locally axisymmetric turbulence. *Journal of Fluid Mechanics*, 233:1–23, 1991.

[16] H. J. Hussein, S. P. Capp, and W. K. George. Velocity measurements in a high-reynolds-number, momentum-conserving, axisymmetric, turbulent jet. *Journal of Fluid Mechanics*, 258:31–75, 1994.

[17] R. Kerr. Comment at workshop on turbulence. In *National Center for Atmospheric Research (Unpublished), Boulder, Colorado*, July 1987.

[18] N. W. M. Ko and W. T. Chan. Similarity in the initial region of annular jets: three configurations. *Journal of Fluid Mechanics*, 84:641–656, 2 1978.

[19] J. Lemay and A. Benaïssa. Improvement of cold-wire response for measurement of temperature dissipation. *Experiments in Fluids*, 31(3):347–356, 2001.

[20] J. Lemay, A. Benaïssa, and A. Darisse. Budgets of turbulent kinetic energy and scalar variance in the self-similar region of a round jet. In *The European turbulence conference 14*, September 2013.

[21] D. D. Papailiou and P. S. Lykoudis. Turbulent vortex streets and the entrainment mechanism of the turbulent wake. *Journal of Fluid Mechanics*, 62:11–31, 1 1974.

[22] P. Paranthoën and J. C. Lecordier. Mesures de temperature dans les écoulements turbulents. *Revue Generale de Thermique*, 35(413):283 – 308, 1996.

[23] W. M. Pitts. Effects of global density ratio on the centerline mixing behavior of axisymmetric turbulent jets. *Experiments in Fluids*, 11(2-3):125–134, 1991.

[24] R. W. Schefer, M. Namazian, J. Kelly, and M. Perrin. Effect of confinement on bluff-body burner recirculation zone characteristics and flame stability. *Combustion Science and Technology*, 120(1-6):185–211, 1996.

[25] F. Thiesset, R. A. Antonia, and L. Djenidi. Consequences of self-preservation on the axis of a turbulent round jet. *Journal of Fluid Mechanics*, 748, 6 2014.

[26] F. Thiesset, R. A. Danaila, L. Antonia, and T. Zhou. Scale-by-scale energy budgets which account for the coherent motion. *Journal of Physics: Conference Series*, 318(5):052040, 2011.

[27] P. V. Vukoslavčević and J. M. Wallace. The simultaneous measurement of velocity and temperature in heated turbulent air flow using thermal anemometry. *Meas. Sci. Technol.*, 13(10):1615, 2002.

[28] H. A. Warda, S. Z. Kassab, K. A. Elshorbagy, and E. A. Elsaadawy. An experimental investigation of the near-field region of a free turbulent coaxial jet using LDA. *Flow Measurement and Instrumentation*, 10(1):15 – 26, 1999.

[29] I. Wygnanski and H. Fiedler. Some measurements in the self-preserving jet. *Journal of Fluid Mechanics*, 38:577–612, 9 1969.